# Online Configuration Selection for Redundant Arrays of Inertial Sensors: Application to Robotic Systems Covered with a Multimodal Artificial Skin

Quentin Leboutet, *Student Member, IEEE,* Florian Bergner, *Student Member, IEEE,*
and Gordon Cheng, *Fellow, IEEE*

*Abstract*— **Multiple approaches to the estimation of high-order motion derivatives for innovative control applications now rely on the data collected by redundant arrays of inertial sensors mounted on robots, with promising results. However, most of these works suffer scalability issues induced by the considerable amount of data generated by such large-scale distributed sensor systems. In this article, we propose a new adaptive sensor-selection algorithm, for distributed inertial measurements. Our approach consists in using the data of a subset of sensors, selected among a larger collection of inertial sensing elements covering a rigid robot link. The sensor selection process is formulated as an optimization problem, and solved using a projected gradient heuristics. The proposed method can run online on a robot and be used to recalculate the selected sensor arrangement on the fly when physical interaction or potential sensor failure is detected. The tests performed on a simulated UR5 industrial manipulator covered with a multimodal artificial skin, demonstrate the consistency and performance of the proposed sensor-selection algorithm.**

*Index Terms*— **Acceleration Feedback, Artificial Robot Skin, Automatic Sensor Selection, Greedy Algorithm**

## I. INTRODUCTION

### A. Motivation and Related Works

Reliable estimation of high-order motion derivatives is of paramount importance in robotics, with significant implications in the fields of control and parameter identification. On a robotic system, motion derivatives such as joint velocities or accelerations are usually computed through sequential time-derivation and filtering of the raw encoder data, yielding substantial amounts of high-frequency noise as well as a non-negligible lag [1]. As a result, the obtained signals generally prove unsuitable for use in high-gain control loops. Driven by the large-scale democratization of very low-cost inertial sensors, referred to as micro-electro-mechanical systems (MEMS) [2], several alternative approaches proposed to fuse the joint encoder data with the derivative-free estimates of the linear and angular components of motion provided by a set of Inertial Measurement Units (IMUs), rigidly attached to the different links of a robot [3]–[10]. In this context, sensor redundancy proves to be of significant interest as it makes it theoretically possible to significantly reduce the measurement noise [11] while at the same time providing enhanced robustness to possible sensor failures through adequate fault

The authors are with the Faculty of Electrical Engineering and Computer Science, Institute for Cognitive Systems, Technical University of Munich, 80333 Munich, Germany (e-mail:quentin.leboutet@tum.de; florian.bergner@tum.de; gordon.cheng@ieee.org).
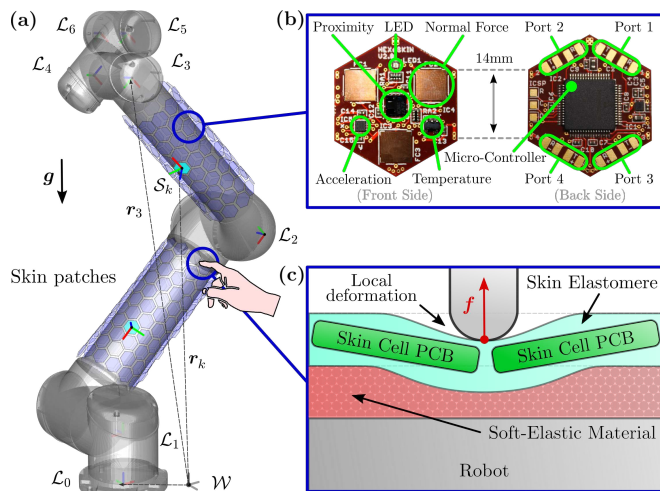
Fig. 1: **(a)**: Our experimental platform is a UR5 industrial robot from Universal robotics, covered with 253 artificial skin cells. **(b)**: The artificial skin mounted on our robot is a redundant network of identical measurement units or "cells" organized in patches of different size. **(c)**: The skin is mounted over a layer of soft-elastic material to better fit the shape of the robot and dampen high-frequency mechanical vibrations. During physical interaction with the external environment, this layer is likely to deform, thereby slightly changing the orientation of the sensor attached to it.

detection and isolation techniques [12]–[15]. In practice, one of the main obstacles to the successful deployment of whole-body distributed inertial feedback in robotics turns out to be the considerable amount of data that can potentially be generated by such a system, especially considering that inertial sensing generally requires high sampling rates. To produce the intended effect on the robot, data must be transmitted and processed in real-time, at the control loop frequency. This is a complex problem, which rapidly becomes intractable when the generated amount of data exceeds the system's bandwidth. Evolutionary processes in nature converged towards a remarkably elegant and effective solution to this issue in the context of tactile perception. By contextualizing the process of data generation, the sensory receptors of the natural skin mainly transmit information that suggests a change of state (e.g., variations in temperature or force) [16]. Accordingly, multiple neuromorphic event-driven approaches to distributed sensing were recently developed, especially

for applications involving massively redundant arrays of sensors, such as artificial robot skins, with promising results [17]–[23]. Although such approaches could potentially be applied to raw inertial data, suitable implementation of the event generation engine usually require a dedicated sensor hardware. In the more general case where distributed sensors can only operate in continuous mode, the issue of data flow limitation can still be adequately addressed, provided that it is treated as a sensor-selection problem, namely finding for each robot link $i$ equipped with a set of $N_i$ inertial sensors, a subset of $M_i$ sensing elements that provide the best compromise in terms of the network load and of an application-relevant metric. Once identified, the selected sensors are set to broadcast measurement at the maximum frequency while other sensors are deactivated or run at a lower update rate. Sensor-selection is a widely studied topic, with multiple contributions, ranging from energy optimization in redundant WiFi networks [24] to distributed state estimation and tracking [25], [26]. Besides network load mitigation, sensor selection has multiple potential uses in robotics. As a matter of fact, most state-of-the-art distributed inertial measurement techniques are based on the assumption that the sensors are rigidly coupled to the robot link to which they are mounted. However this assumption is not always verified in practice, considering that the sensors that come into direct contact with the external environment are likely to undergo local deformations and impacts, which in turn induces inconsistencies into the inertial measurements collected by the system (c.f. Fig. 1.c). In this context the ability to reorganize the sensor network online, discarding the corrupted elements, would prove invaluable. However, for this to be achievable, this re-organization step must be done as fast as possible. Sensor-selection is often considered as a NP-hard combinatorial optimization problem [27]. As a result, the approaches to solving the sensor-selection problems are essentially application-specific [28]. If the accuracy of the result is of prime importance, global optimization techniques will be considered, regardless of the required computational effort. This is for example the case in [29] where a branch-and-bound method is presented. However if the considered application is subject to strict constraints in terms of timing or computational power, as it is often the case in robotics, local sub-optimal heuristic approaches will be preferred as for example proposed in [30] based on convex optimization techniques or in [31], [32] using tailor-made greedy algorithms.

### B. Our Approach and Contribution

In this paper, we propose a new online sensor selection algorithm allowing to automatically determine suitable combinations of inertial sensors, for robot links acceleration estimation purposes. We consider the case of a UR5 industrial robot, covered with a multimodal artificial skin. The skin is a redundant network of interconnected sensing units or "*cells*". It is organized in patches of different sizes (see Fig.1) and provides continuous measurements of the normal contact forces, proximity, temperature and three-dimensional accelerations, at the cells mounting points [23], [33], [34]. Although multiple approaches already tackled the problem of inertial sensor *placement*, in particular in the context of gyroscope-free navigation [35]–[43], the issue of inertial sensor *selection* among larger redundant sets with fixed geometries is seldom addressed. Similarly to [30], our approach does not intend to find the globally optimal sensor configuration, but rather focuses on providing a "sufficiently good" sub-optimal configuration, fast enough to allow online implementation and adaptation on a robot. We formulate the sensor selection problem as a greedy algorithm, guided by a locally projected gradient heuristics. The adaptability of our approach stems from the fact that we can use the precontact information provided by the proximity sensors of the artificial skin in order to automatically trigger a re-computation of the sensor configuration, excluding the cells and neighbors that are likely to get into contact with the external environment. The present paper is organized as follows: in Section II we provide a formal description of the redundant distributed inertial sensing problem. Section III describes the proposed approach for online sensor selection on a robot covered with artificial skin. The numerical simulations performed on a model of UR5 industrial robot manipulator, are presented and their results are discussed in Section IV. Finally, Section V gives a brief conclusion and discusses future works.

## II. REDUNDANT DISTRIBUTED INERTIAL SENSING

### A. Fundamentals of Distributed Inertial Sensing

We consider the movements of a rigid robot link $i$ in an inertial reference frame $\mathcal{W}$, as depicted in Fig. 1.a. The link $i$ is equipped with a set of $N_i$ triple-axis acceleration sensors, spatially distributed and rigidly coupled to as many different mounting points. Each sensor $k = \{1 \cdots N_i\}$ of the link $i$ measures a linear acceleration ${}^{\mathcal{S}_k}\boldsymbol{a}_k$ in a body-attached sensor reference frame $\mathcal{S}_k$:

$$ {}^{\mathcal{S}_k}\boldsymbol{a}_k = \boldsymbol{R}_{\mathcal{W}}^{\mathcal{S}_k}\left(\boldsymbol{a}_k + \boldsymbol{g}\right) + {}^{\mathcal{S}_k}\boldsymbol{b}_k + {}^{\mathcal{S}_k}\boldsymbol{n}_k \in \mathbb{R}^3. \quad (1) $$

In this expression, $\boldsymbol{g} = [0\ 0\ -9.81]^\top\ m.s^{-2}$ denotes the gravitational acceleration and $\boldsymbol{a}_k \in \mathbb{R}^3$ the acceleration induced by the robot movements. The terms ${}^{\mathcal{S}_k}\boldsymbol{b}_k \in \mathbb{R}^3$ and ${}^{\mathcal{S}_k}\boldsymbol{n}_k \sim \mathcal{N}(\boldsymbol{0}_{3\times 1}, \boldsymbol{\sigma}_a)$ respectively denote the sensor bias and noise vectors while $\boldsymbol{R}_{\mathcal{W}}^{\mathcal{S}_k} \in \boldsymbol{SO}(3)$ is the rotation matrix relating the sensor frame $\mathcal{S}_k$ to the inertial frame $\mathcal{W}$. The acceleration $\ddot{\boldsymbol{x}}_i = [\boldsymbol{v}_i^\top,\ \dot{\boldsymbol{\omega}}_i^\top]^\top \in \mathbb{R}^6$ of a link-attached coordinate frame $\mathcal{L}_i$ can be related to the acceleration $\boldsymbol{a}_k$ of any sensor frame $\mathcal{S}_k$ through the following expression:

$$ \underbrace{\boldsymbol{a}_k}_{\substack{\text{Sensor frame}\\\text{acceleration}}} = \underbrace{\dot{\boldsymbol{v}}_i}_{\substack{\text{Link frame}\\\text{acceleration}}} + \underbrace{\boldsymbol{\omega}_i \times \left(\boldsymbol{\omega}_i \times \boldsymbol{r}_i^k\right)}_{\substack{\text{Centrifugal}\\\text{acceleration}}} + \underbrace{\dot{\boldsymbol{\omega}}_i \times \boldsymbol{r}_i^k}_{\substack{\text{Euler}\\\text{acceleration}}}, \quad (2) $$

where $\boldsymbol{r}_i^k = \boldsymbol{r}_k - \boldsymbol{r}_i \in \mathbb{R}^3$ denotes the position of the sensor frame $\mathcal{S}_k$ relative to the joint frame $\mathcal{L}_i$, expressed in the coordinate system of $\mathcal{W}$, and $\forall \boldsymbol{u}, \boldsymbol{v} \in \mathbb{R}^3, \boldsymbol{u} \times \boldsymbol{v}$ denotes the cross-product between vectors $\boldsymbol{u}$ and $\boldsymbol{v}$.

## B. Fusion of the Redundant Skin Acceleration Measurements

One of the most widely used approach to fusion of redundant acceleration measurements, often referred to as *accelerometer-only* or *gyroscope-free* IMU (AO-IMU resp. GF-IMU), is based solely on the measurement of multiple acceleration sensors, mounted in different places on the same rigid body. This allows rewriting (2) in the form of a linear system, as for instance proposed in [44]–[46]:

$$\boldsymbol{a}_k = \boldsymbol{G}_i^k \boldsymbol{\psi}_i. \tag{3}$$

where $\boldsymbol{\psi}_i = \begin{bmatrix} \dot{\boldsymbol{v}}_i^\top & \dot{\boldsymbol{\omega}}_i^\top & \begin{bmatrix} \omega_x^2 & \omega_y^2 & \omega_z^2 & \omega_x\omega_y & \omega_y\omega_z & \omega_z\omega_x \end{bmatrix}^\top \end{bmatrix}^\top \in \mathbb{R}^{12}$ is referred to as the augmented state vector while $\boldsymbol{G}_i^k = \begin{bmatrix} \boldsymbol{I}_{3\times3} & -\boldsymbol{S}(\boldsymbol{r}_i^k) & -\boldsymbol{S}(\dot{\boldsymbol{r}}_i^k) & \boldsymbol{B}(\boldsymbol{r}_i^k) \end{bmatrix} \in \mathbb{R}^{3\times12}$ denotes the associated observation matrix. $\forall \boldsymbol{u}, \boldsymbol{v} \in \mathbb{R}^3$, we define the cross product operator $\boldsymbol{S}(\cdot) \in \mathbb{R}^{3\times3}$ as $\boldsymbol{S}(\boldsymbol{u})\boldsymbol{v} = \boldsymbol{u} \times \boldsymbol{v}$, and $\boldsymbol{B}(\boldsymbol{u}) = \begin{bmatrix} 0 & -u_x & -u_x & u_y & 0 & u_z \\ -u_y & 0 & -u_y & u_x & u_z & 0 \\ -u_z & -u_z & 0 & 0 & u_y & u_x \end{bmatrix} \in \mathbb{R}^{3\times6}$.
Therefore, determining the linear and angular acceleration of a rigid body from distributed inertial measurements simply amounts to solve an inverse problem. In practice, obtaining a unique solution to this problem requires to stack the measurements of at least four triads of acceleration sensors into an augmented vector $\boldsymbol{y} = \begin{bmatrix} \boldsymbol{a}_1^\top \cdots \boldsymbol{a}_{N_i}^\top \end{bmatrix}^\top \in \mathbb{R}^{3N_i}$. Inverting the corresponding augmented observation matrix $\boldsymbol{G}_i = [\boldsymbol{G}_i^{1\top} \cdots \boldsymbol{G}_i^{N_i\top}]^\top \in \mathbb{R}^{3N_i\times12}$ using a left psedoinverse, leads to the least-squares body acceleration estimate:

$$\boldsymbol{\psi}_i = (\boldsymbol{G}_i^\top \boldsymbol{G}_i)^{-1} \boldsymbol{G}_i^\top \boldsymbol{y}, \tag{4}$$

Despite its relative simplicity, this method has several disadvantages, limiting its use in robotics or navigation applications. These limitations stem in particular from the sign ambiguity[1] on $\boldsymbol{\omega}_i$, and from poor performances at low angular velocities as the cetrifugal acceleration term in (2) cannot be suitably measured due to the limited resolution of the accelerometers [47]. An alternative approach, introduced in [48], consists in reformulating (2) as the sum of a linear and non-linear term:

$$\boldsymbol{a}_k = \dot{\boldsymbol{v}}_i + \left( \boldsymbol{S}^2(\boldsymbol{\omega}_i) + \boldsymbol{S}(\dot{\boldsymbol{\omega}}_i) \right) \boldsymbol{r}_i^k \tag{5a}$$

$$= \underbrace{\begin{bmatrix} \boldsymbol{I}_{3\times3} & -\boldsymbol{S}(\boldsymbol{r}_i^k) \end{bmatrix}}_{\boldsymbol{H}_i^k} \underbrace{\begin{bmatrix} \dot{\boldsymbol{v}}_i \\ \dot{\boldsymbol{\omega}}_i \end{bmatrix}}_{\ddot{\boldsymbol{x}}_i} + \underbrace{\boldsymbol{S}^2(\boldsymbol{\omega}_i)\boldsymbol{r}_i^k}_{\boldsymbol{h}_i^k(\boldsymbol{\omega}_i)}. \tag{5b}$$

Provided that a suitable measure of $\boldsymbol{\omega}_i$ is available, which is usually the case on a fixed robot manipulator using the encoder data or a set of body-attached gyroscopes, the linear and angular acceleration terms $\dot{\boldsymbol{v}}_i$ and $\dot{\boldsymbol{\omega}}_i$ of link $i$ can also be obtained using a weighted left pseudo-inverse:

$$\ddot{\boldsymbol{x}}_i = \begin{bmatrix} \dot{\boldsymbol{v}}_i \\ \dot{\boldsymbol{\omega}}_i \end{bmatrix} = \left( \boldsymbol{H}_i^\top \boldsymbol{Q}^{-1} \boldsymbol{H}_i \right)^{-1} \boldsymbol{H}_i^\top \boldsymbol{Q}^{-1} \left( \boldsymbol{y} - \boldsymbol{h}_i(\boldsymbol{\omega}_i) \right) \tag{6}$$

---

[1]The sign ambiguity on the angular velocity term stems from its quadratic nature within the vector $\boldsymbol{\psi}_i$. This is a direct consequence of the centrifugal acceleration term in (2).

where $\boldsymbol{H}_i = \begin{bmatrix} \boldsymbol{H}_i^{1\top} \cdots \boldsymbol{H}_i^{N_i\top} \end{bmatrix}^\top \in \mathbb{R}^{3N_i\times6}$ and $\boldsymbol{h}_i(\boldsymbol{\omega}_i) = \begin{bmatrix} \boldsymbol{h}_i^1(\boldsymbol{\omega}_i)^\top \cdots \boldsymbol{h}_i^{N_i}(\boldsymbol{\omega}_i)^\top \end{bmatrix}^\top \in \mathbb{R}^{3N_i}$ are respectively the augmented observation matrix and the centrifugal acceleration vector. The covariance matrix $\boldsymbol{\Sigma}_i \in \mathbb{R}^{6\times6}$ of the acceleration estimate (6) can be expressed as $\boldsymbol{\Sigma}_i = (\boldsymbol{H}_i^\top \boldsymbol{Q}^{-1} \boldsymbol{H}_i)^{-1}$, where the matrix $\boldsymbol{Q} \in \mathbb{R}^{3N_i\times3N_i}$ denotes the acceleration sensors' noise covariance matrix, here assumed to be diagonal and measured directly. Among the most significant advantages of this approach over the previous one are its compatibility with 2D flat sensor geometries, as described in [48], and the fact that it still provides reliable measurements in the low angular velocity range[2].

## III. ONLINE SENSOR SELECTION ALGORITHM

### A. Value function for Distributed Inertial Sensor Selection

Since the fusion of spatially-separated inertial measurements can be considered as an inverse problem, the result is, therefore, intrinsically dependent on the conditioning of the corresponding observation matrix. As the latter is a function of the geometric arrangement of the sensor array, it can be used as a value function and optimized by modifying the selection vector or the sensor placement in space. Previous work in the context of gyro-free navigation [39] demonstrated that the best results in this respect were obtained when the acceleration sensors were located on the vertices of a platonic solid, as in this case, the observation matrix turns out to be isotropic, i.e., with a unitary condition number. Another relevant figure of merit for our application, and more generally for consumer MEMS-based distributed inertial sensor networks, is the measurement noise mitigation capability. This can be interpreted as minimizing the volume of the confidence ellipsoid of the estimate [37], [38], [42], which is actually proportional to the square-root of the determinant of the covariance matrix $\boldsymbol{\Sigma}_i$. In this work, we decided to make a compromise between these two metrics and defined the value function $f(\boldsymbol{z}_i) : \mathbb{R}^{3\times M_i} \to \mathbb{R}_+$ of the robot link $i$ as a weighted sum of these two terms, namely:

$$f(\boldsymbol{z}_i) = \alpha \cdot \text{cond}(\boldsymbol{\Sigma}_i^{-1}(\boldsymbol{z}_i)) + \beta \cdot \sqrt{\det(\boldsymbol{\Sigma}_i(\boldsymbol{z}_i))} \tag{7}$$

where $\alpha, \beta \in \mathbb{R}_+$ are heuristically determined tuning coefficients, that are here set to $\alpha = 10^{-4}, \beta = 1$ to emphasize the noise attenuation characteristics while penalizing badly conditioned configurations, where $\text{cond}(\boldsymbol{\Sigma}_i^{-1}(\boldsymbol{z}_i)) >> 1$.

### B. Projected Gradient Heuristics

The task of selecting $M_i$ distinct sensing elements among a larger finite set of $N_i$ sensors can be formulated as a combinatorial optimization problem, of the form:

$$\boldsymbol{z}_i^\star = \underset{\boldsymbol{z}_i}{\text{argmin}} \, f(\boldsymbol{z}_i), \quad \text{s.t.} \quad \boldsymbol{1}_{N_i}^\top \boldsymbol{z}_i = M_i \tag{8}$$

where $\boldsymbol{z}_i \in \{0,1\}^{N_i}$ is a Boolean sensor selection vector and $f(\boldsymbol{z}_i) : \{0,1\}^{N_i} \to \mathbb{R}_+$ is an application-dependent value function. Although solving such a problem is in theory

---

[2]This is verified in practice as the noise level of gyroscopes and joint encoders is several orders of magnitude lower than that of accelerometers.
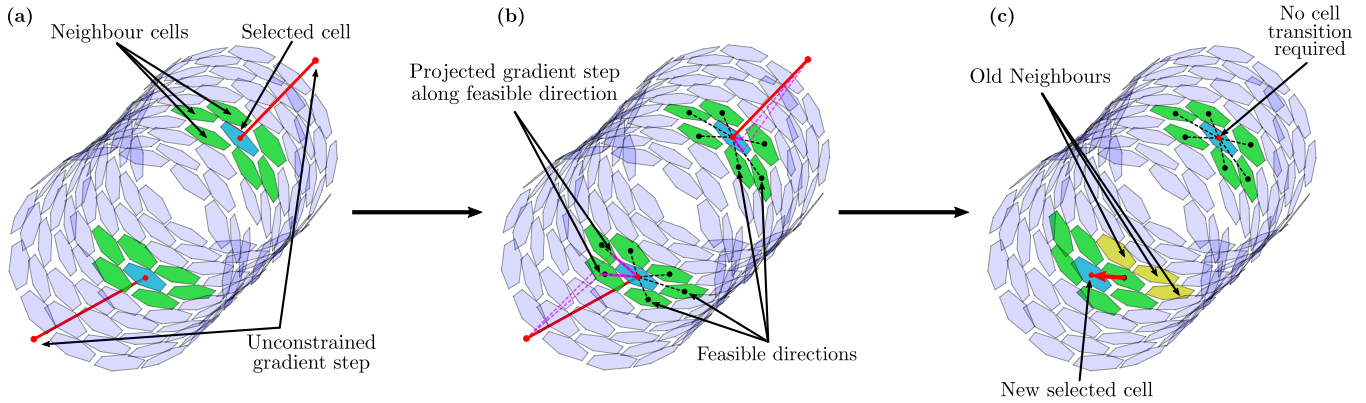
Fig. 2: One iteration of the proposed algorithm on two cells of the upper-arm patch. The idle cells are depicted in blue, while the selected cells broadcasting information at the maximum frequency, and their neighbors are depicted in cyan and green respectively. The unconstrained gradient step is represented as a red segment and its projection along feasible directions of the problem is depicted in magenta. **(a)**: First the neighbors of each selected cells are extracted and a classic gradient step of the unconstrained problem is computed. **(b)**: The unconstrained gradient step is then projected along each feasible direction. The highest norm projection is then selected. **(c)**: If the norm of this gradient projection is greater than a heuristically defined threshold $\zeta$, then a cell-switch event is triggered with the corresponding neighbor cell along the selected direction.

feasible by brute-forcing every possible sensor combination, this proves intractable in practice this number grows with binomial coefficient of $M_i$ and $N_i$. In this paper, the proposed heuristic to minimizing (7) is formulated as a projected gradient descent. From an initial random sensor distribution on the robot link $i$, we proceed by first computing the gradient $\nabla_{\boldsymbol{r}_i(\boldsymbol{z}_i)} f(\boldsymbol{z}_i)$ of the value function $f(\boldsymbol{z}_i)$ in terms of the selected sensors Cartesian coordinate vectors $\boldsymbol{r}_i(\boldsymbol{z}_i) \in \mathbb{R}^{3 \cdot M_i}$, relative to the link frame $\mathcal{L}_i$. The following gradient step is then derived for each selected sensor $k$, regardless of the patch geometrical constraints (c.f. Fig. 2.a):

$$\hat{\boldsymbol{r}}_i^k = \boldsymbol{r}_i^k - \eta \nabla_{\boldsymbol{r}_i^k} f(\boldsymbol{z}) \qquad (9)$$

where $\eta \in \mathbb{R}_+$ is a tuning parameter. This unconstrained gradient step is then projected onto the constrained Cartesian subspace $\mathcal{E}_i^k$ of the problem. We define the subspace $\mathcal{E}_i^k$ in a cell-wise manner, as the set of unit-length segments directed along the cell-to-neighbor vectors $\boldsymbol{r}_i^{k,n_k} = \boldsymbol{r}_i^{n_k} - \boldsymbol{r}_i^k$ as depicted in Fig. 2.b. For each selected cell, the neighbor $n_k^\star$ of cell $k$ with the maximal projection value will be labeled as *candidate*, to be considered for the next algorithm iteration:

$$n_k^\star = \operatorname{argmax}(\operatorname{Proj}_{\mathcal{E}_i^k}(\hat{\boldsymbol{r}}_i^k - \boldsymbol{r}_i^k)) \in \mathbb{R} \qquad (10)$$

The different candidates are then filtered such that:

1) only the candidates whose projected norm is greater than a predefined threshold $\rho \in \mathbb{R}_+$ are declared valid and used (c.f. Fig. 2.c),
2) the candidates whose index belong to the set of "unusable cells", namely the sensors that are identified as malfunctioning, undergoing physical interaction[3], or that are already selected in the current iteration are automatically discarded. The vector containing these indexes is automatically updated at each control period.

---

[3]In this work, we identify unusable cells by exploiting the multi-modality of the skin, making use of the proximity and force sensors to determine precontact and contact conditions.

At the end of these two filtering steps, the remaining cell candidates define the new selected sensor set. The whole process is repeated until convergence, when the vector of filtered candidates turns out to be empty.

## IV. VALIDATION BY NUMERICAL SIMULATION

### A. Description of the Validation Setup and Protocol

The validation setup is presented in Fig. 1. We consider a model of 6-DoF UR5 industrial robot arm from Universal robotics, covered with two patches of artificial skin, accounting for a total of 253 cells. Cell positions and orientations were determined using calibration data, obtained from the actual skin system mounted on a real UR5. We used the self-configuration procedure detailed in [49]. The proposed validation protocol consists of two main steps. We first analyze the convergence properties of our method and compare them to that of a greedy algorithm by executing a Monte Carlo Simulation (MCS) on a set of randomly generated initial cell configurations ranging from 3 to 20 cells. Note that since a set of at least three cells is required to get reliable acceleration estimates using (6), the greedy algorithm has to be initialized with a non-empty cell distribution, which, in this work, is either randomly generated or computed using the proposed projected gradient algorithm from a random initial set. Here the randomly initialized greedy is referred to as "*standard*" while the projected-gradient-initialized greedy is referred to as "*hot-started*". The second validation step aims at demonstrating the performance gain, in term of measurement noise mitigation, along a predefined trajectory executed by a simulated UR5 robot. The fact that this phase is executed in simulation is here justified by the need of a noiseless link acceleration reference and of perfectly-calibrated acceleration sensors, for suitable assessment of the estimation quality. During this experiment, a simulated UR5 robot tracks a preset trajectory, defined as a weighted sum of sinusoids. Two sets
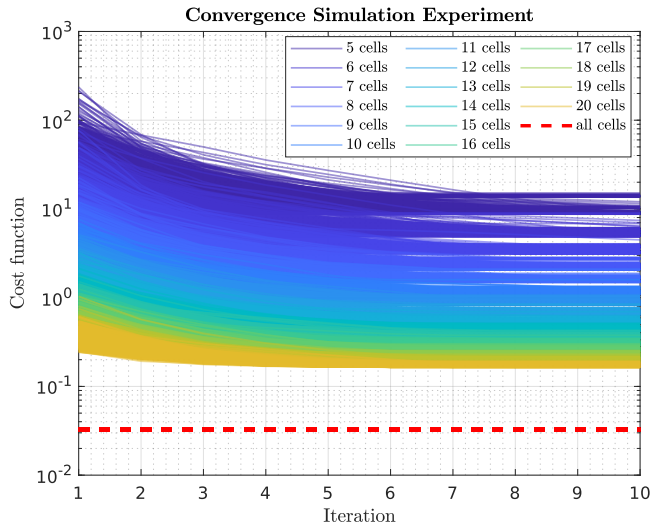
(a) Convergence of our method over $10^4$ randomly generated initial cell configurations of 5 to 20 cells. The red-dashed line corresponds to the value function when all the cells are activated.
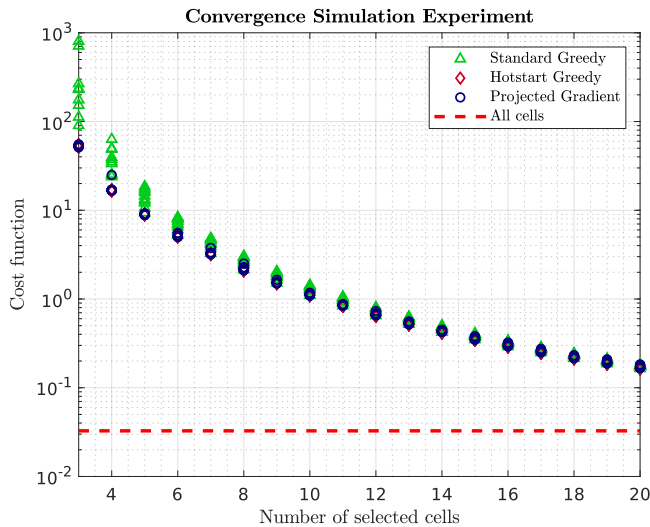


(b) Comparison over 10 randomly generated initial cell configurations of 3 to 20 cells, of the convergence of our method with a standard greedy algorithm and a "hotstart" greedy algorithm.

Fig. 3: Convergence results

of simulated skin cells, rigidly coupled to the robot body, measure the 3D acceleration along this trajectory. As for actual accelerometers, a normally distributed measurement noise with standard deviation $\sigma = 0.34 \cdot \boldsymbol{I}_{3 \times 3}$[4] is added to the acceleration measurements of each simulated skin cell. Estimates of the link linear and angular accelerations are then computed using (6) and the skin acceleration data acquired with different cell numbers and configurations. In practice, these configurations are generated, on the one hand, using our method and, on the other hand, using the standard and hot-started greedy algorithms. We compare the estimated link accelerations to the reference accelerations computed using the closed form expressions of the robot second order kinematics and use the variance of the difference between these two signals as a noise-level metric.

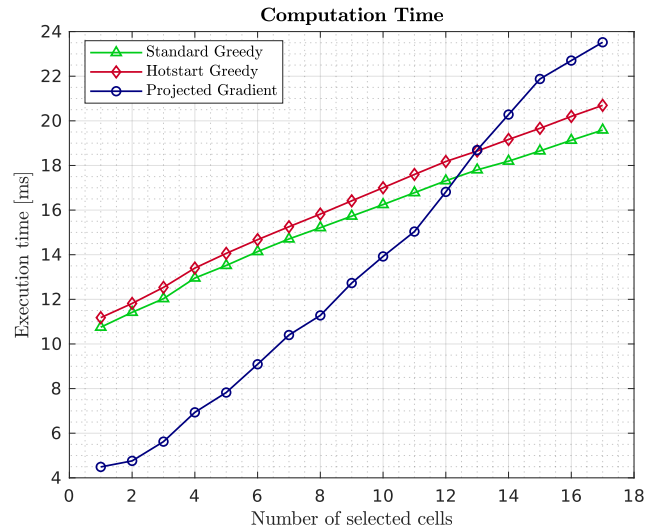[4]This value was determined from actual sensor measurements.



Fig. 4: Mean execution time of our method, vs standard and hot-started greedy over $10^3$ randomly generated initial cell configurations of 5 to 20 cells each.

### B. Results and Discussion

The results of the convergence experiment are displayed in Figs. 3a, 3b and Fig. 4. From Fig. 3a, it is possible to see that convergence of the proposed algorithm is achieved in less than ten iterations. Nevertheless Fig. 3a reveals a non-negligible spread in the final cost values for a given number of cells, thereby suggesting a lack of robustness of the proposed algorithm to local minima. Note that the effects of unusable cells does not noticeably appear in this study and would deserve deeper treatment. This is here considered as future works. Fig. 3b suggest that the quality of the resulting optimizer exceeds that of the standard greedy for cell numbers ranging from three to fifteen. This can be explained by the random nature of the initial cell distribution used in this algorithm. It is interesting to note that the performances of our algorithm are similar to those of the greedy algorithm when the latter is hot-started with an optimized initial distribution. One of the main advantages of the proposed method lies in its execution time. This is clearly visible in Fig. 4, where we can see that our algorithm is up to two times faster than greedy algorithms for sets of three to thirteen cells, which generally corresponds to the number of sensing elements used on the links of a robot, as it offers a good compromise between network load and measurement accuracy. The mean convergence time is evaluated to 10.5ms on Matlab for 7-cells in a 144 cells patch, which is compatible with online use, considering in particular that for loops run much faster in C++. Execution of our sensor selection algorithm on an actual skin system, mounted on a real UR5 robot proved its reactivity and ability to run online, at the robot control interface frequency (i.e. 125Hz on the UR5). The results are shown in the attached video. The results of the noise mitigation experiment are displayed in Figs.5 and 6 in terms of the linear accelerations measured on the second link using (6). Fig.5 shows in particular the consequences of an ill-selected cell configuration, referred to as "grouped" and

**Linear Acceleration Data, Grouped Cell Configuration**

**Linear Acceleration Data, Optimized Cell Configuration**

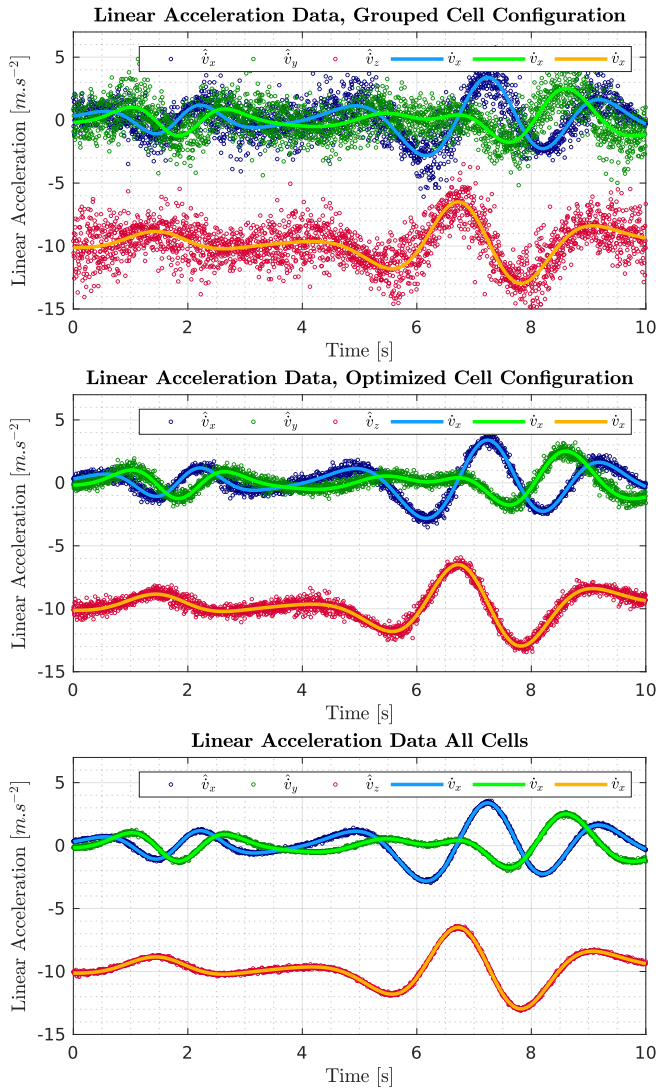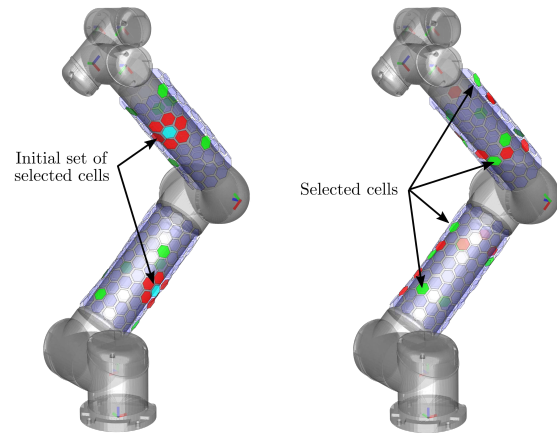**Linear Acceleration Data All Cells**

Fig. 5: Linear accelerations of the second link of a simulated UR5 manipulator. The estimated values $\hat{v}_x, \hat{v}_y, \hat{v}_z$ computed using (6) and the measurements of 7 skin cells in three different configurations, namely *grouped* (c.f. Fig.6a), *optimized* and *full-set*, are compared to the reference values $\dot{v}_x, \dot{v}_y, \dot{v}_z$.



(a) A set of initial (red) and final (green) cell configurations on the simulated UR5 manipulator during a validation run. On the left, a grouped initial configuration of seven cells. On the right, a randomly distributed initial configuration of seven cells.



**Noise Level in Linear Accelertion Estimate**

(b) Noise variances obtained with multiple optimized cell configurations over a 10-sample MCS.

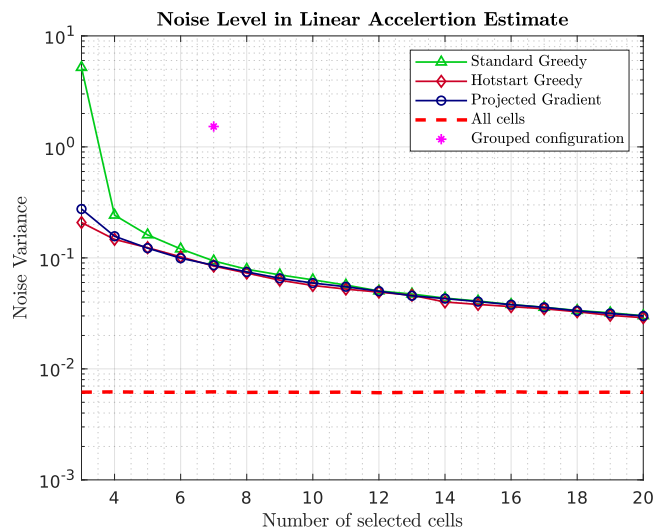Fig. 6: Noise levels for grouped and optimized cell distributions

visible in Fig.6a. The noise variance in this case is depicted as a magenta star marker on Fig.6b. The benefits of the proposed cell selection algorithm in terms of measurement noise attenuation are clearly visible in the middle plot of Fig. 5 and in Fig.6b. Again, it is worth noting the similarity of these results with those of the greedy algorithms.

## V. CONCLUSION

In this work, we proposed a new method for online sensor selection within redundant arrays of inertial measurement units. Relying on a projected gradient heuristics, the proposed sensor selection method is capable of converging in less than ten iterations to new inertial sensor configurations that significantly reduce noise levels in the obtained acceleration estimates. Future work will consist in testing the presented method on a real manipulator and eventually extending it to an entire humanoid robot.

## REFERENCES

[1] F. Nori, S. Traversaro, and M. Fallon, "Sensor fusion and state estimation of the robot," Humanoid Robotics: A Reference, pp. 1–29, 2018.

[2] M. Perlmutter and L. Robin, "High-performance, low cost inertial mems: A market in motion!," in Proceedings of the 2012 IEEE/ION Position, Location and Navigation Symposium, pp. 225–229, IEEE, 2012.

[3] J.-O. Nilsson and I. Skog, "Inertial sensor arrays-a literature review," in Navigation Conference (ENC), 2016 European, pp. 1–10, IEEE, 2016.

[4] X. Xinjilefu, S. Feng, and C. G. Atkeson, "A distributed mems gyro network for joint velocity estimation," in Robotics and Automation (ICRA), 2016 IEEE International Conference on, pp. 1879–1884, IEEE, 2016.

[5] N. Rotella, S. Mason, S. Schaal, and L. Righetti, "Inertial sensor-based humanoid joint state estimation," in Robotics and Automation (ICRA), 2016 IEEE International Conference on, pp. 1825–1831, IEEE, 2016.

[6] X. Zhang, E. Peltola, and J. Mattila, "Joint angle estimation for floating base robots utilizing mems imus," in 2017 IEEE International Conference on Cybernetics and Intelligent Systems (CIS) and IEEE Conference on Robotics, Automation and Mechatronics (RAM), pp. 282–287, IEEE, 2017.

[7] J. Vihonen, J. Mattila, and A. Visa, "Joint-space kinematic model for gravity-referenced joint angle estimation of heavy-duty manipulators," IEEE Transactions on Instrumentation and Measurement, vol. 66, no. 12, pp. 3280–3288, 2017.

[8] X. Zhang, E. Peltola, and J. Mattila, "Angle estimation for robotic arms on floating base using low-cost imus," in 2018 IEEE International Conference on Robotics and Automation (ICRA), pp. 1458–1465, IEEE, 2018.

[9] L. McLean, High-Order Robotic Joint Sensing with Multiple Accelerometer and Gyroscope Systems. PhD thesis, 2018.

[10] Q. Leboutet, J. R. Guadarrama-Olvera, F. Bergner, and G. Cheng, "Second-order kinematics for floating-base robots using the redundant acceleration feedback of an artificial sensory skin," in Robotics and Automation (ICRA), 2020 IEEE International Conference on, pp. XXXX–XXXX, IEEE, 2020.

[11] A. Waegli, J. Skaloud, S. Guerrier, M. E. Parés, and I. Colomina, "Noise reduction and estimation in multiple micro-electro-mechanical inertial systems," Measurement Science and Technology, vol. 21, no. 6, p. 065201, 2010.

[12] K. C. . Daly, E. Gai, and J. V. Harrison, "Generalized likelihood test for fdi in redundant sensor configurations," Journal of Guidance and Control, vol. 2, no. 1, pp. 9–17, 1979.

[13] D.-S. Shim and C.-K. Yang, "Optimal configuration of redundant inertial sensors for navigation and fdi performance," Sensors, vol. 10, no. 7, pp. 6497–6512, 2010.

[14] I. Skog, J.-O. Nilsson, and P. Händel, "An open-source multi inertial measurement unit (mimu) platform," in 2014 International Symposium on Inertial Sensors and Systems (ISISS), pp. 1–4, IEEE, 2014.

[15] T. Brunner, S. Changey, J. P. Lauffenburger, and M. Basset, "Multiple mems-imu localization: Architecture comparison and performance assessment," ICINS, 2015, 2015.

[16] S.-C. Liu and T. Delbruck, "Neuromorphic sensory systems," Current opinion in neurobiology, vol. 20, no. 3, pp. 288–295, 2010.

[17] S. Caviglia, M. Valle, and C. Bartolozzi, "Asynchronous, event-driven readout of posfet devices for tactile sensing," in Circuits and Systems (ISCAS), 2014 IEEE International Symposium on, pp. 2648–2651, IEEE, 2014.

[18] S. Caviglia, L. Pinna, M. Valle, and C. Bartolozzi, "An event-driven posfet taxel for sustained and transient sensing," in Circuits and Systems (ISCAS), 2016 IEEE International Symposium on, pp. 349–352, IEEE, 2016.

[19] W. W. Lee, S. L. Kukreja, and N. V. Thakor, "A kilohertz kilotaxel tactile sensor array for investigating spatiotemporal features in neuromorphic touch," in Biomedical Circuits and Systems Conference (BioCAS), 2015 IEEE, pp. 1–4, IEEE, 2015.

[20] F. Bergner, P. Mittendorfer, E. Dean-Leon, and G. Cheng, "Event-based signaling for reducing required data rates and processing power in a large-scale artificial robotic skin," in Intelligent Robots and Systems (IROS), 2015 IEEE/RSJ International Conference on, pp. 2124–2129, IEEE, 2015.

[21] F. Bergner, E. Dean-Leon, and G. Cheng, "Event-based signaling for large-scale artificial robotic skin-realization and performance evaluation," in Intelligent Robots and Systems (IROS), 2016 IEEE/RSJ International Conference on, pp. 4918–4924, IEEE, 2016.

[22] F. Bergner, E. Dean-Leon, and G. Cheng, "Efficient event-driven reactive control for large scale robot skin," in Robotics and Automation (ICRA), 2017 IEEE International Conference on, pp. 394–400, IEEE, 2017.

[23] G. Cheng, E. Dean-Leon, F. Bergner, J. R. G. Olvera, Q. Leboutet, and P. Mittendorfer, "A comprehensive realization of robot skin: Sensors, sensing, control, and applications," Proceedings of the IEEE, vol. 107, no. 10, pp. 2034–2051, 2019.

[24] H. Rowaihy, S. Eswaran, M. Johnson, D. Verma, A. Bar-Noy, T. Brown, and T. La Porta, "A survey of sensor selection schemes in wireless sensor networks," in Unattended Ground, Sea, and Air Sensor Technologies and Applications IX, vol. 6562, p. 65621A, International Society for Optics and Photonics, 2007.

[25] P. Chavali and A. Nehorai, "Scheduling and power allocation in a cognitive radar network for multiple-target tracking," IEEE Transactions on Signal Processing, vol. 60, no. 2, pp. 715–729, 2011.

[26] S. P. Chepuri and G. Leus, "Sparsity-promoting sensor selection for non-linear measurement models," IEEE Transactions on Signal Processing, vol. 63, no. 3, pp. 684–698, 2014.

[27] F. Bian, D. Kempe, and R. Govindan, "Utility based sensor selection,"

in Proceedings of the 5th international conference on Information processing in sensor networks, pp. 11–18, 2006.

[28] A. O. Hero and D. Cochran, "Sensor management: Past, present, and future," IEEE Sensors Journal, vol. 11, no. 12, pp. 3064–3075, 2011.

[29] W. J. Welch, "Branch-and-bound search for experimental designs based on d optimality and other criteria," Technometrics, vol. 24, no. 1, pp. 41–48, 1982.

[30] S. Joshi and S. Boyd, "Sensor selection via convex optimization," IEEE Transactions on Signal Processing, vol. 57, no. 2, pp. 451–462, 2008.

[31] M. Shamaiah, S. Banerjee, and H. Vikalo, "Greedy sensor selection: Leveraging submodularity," in 49th IEEE conference on decision and control (CDC), pp. 2572–2577, IEEE, 2010.

[32] A. Hashemi, M. Ghasemi, H. Vikalo, and U. Topcu, "A randomized greedy algorithm for near-optimal sensor scheduling in large-scale sensor networks," in 2018 Annual American Control Conference (ACC), pp. 1027–1032, IEEE, 2018.

[33] P. Mittendorfer and G. Cheng, "Humanoid multimodal tactile-sensing modules," Robotics, IEEE Transactions on, vol. 27, no. 3, pp. 401–410, 2011.

[34] P. Mittendorfer, From a Multi-modal Intelligent Cell to a Self-organizing Robotic Skin-Realizing Self and Enriching Robot Tactile Interaction. PhD thesis, Technische Universität München, 2015.

[35] T. Williams and K. Fyfe, "Planar accelerometer configurations," Journal of applied mechanics, vol. 71, no. 1, pp. 10–14, 2004.

[36] P. Cardou and J. Angeles, "Singularity analysis of accelerometer strapdowns for the estimation of the acceleration field of a planar rigidbody motion," in Proceedings of the 12th World Congress in Mechanism and Machine Science, 2007.

[37] M. Jafari and J. Roshanian, "Optimal redundant sensor configuration for accuracy and reliability increasing in space inertial navigation systems," The Journal of Navigation, vol. 66, no. 2, pp. 199–208, 2013.

[38] M. Jafari, "Optimal redundant sensor configuration for accuracy increasing in space inertial navigation system," Aerospace Science and Technology, vol. 47, pp. 467–472, 2015.

[39] Z. Qin, L. Baron, and L. Birglen, "Robust design of inertial measurement units based on accelerometers," Journal of Dynamic Systems, Measurement, and Control, vol. 131, no. 3, p. 031010, 2009.

[40] B. Zappa, G. Legnani, A. J. Van Den Bogert, and R. Adamini, "On the number and placement of accelerometers for angular velocity and acceleration determination," Transactions-American Society of Mechanical Engineers, Journal of Dynamic Systems Measurement and Control, vol. 123, no. 3, pp. 552–553, 2001.

[41] G. Baselli, G. Legnani, P. Franco, F. Brognoli, A. Marras, F. Quaranta, and B. Zappa, "Assessment of inertial and gravitational inputs to the vestibular system," Journal of Biomechanics, vol. 34, no. 6, pp. 821–826, 2001.

[42] J. W. Song and C. G. Park, "Optimal configuration of redundant inertial sensors considering lever arm effect," IEEE Sensors Journal, vol. 16, no. 9, pp. 3171–3180, 2016.

[43] N. Sahu, P. Babu, A. Kumar, and R. Bahl, "A novel algorithm for optimal placement of multiple inertial sensors to improve the sensing accuracy," IEEE Transactions on Signal Processing, vol. 68, pp. 142–154, 2019.

[44] S. Park and S. K. Hong, "Angular rate estimation using a distributed set of accelerometers," Sensors, vol. 11, no. 11, pp. 10444–10457, 2011.

[45] S. O. Madgwick, A. J. Harrison, P. M. Sharkey, R. Vaidyanathan, and W. S. Harwin, "Measuring motion with kinematically redundant accelerometer arrays: Theory, simulation and implementation," Mechatronics, vol. 23, no. 5, pp. 518–529, 2013.

[46] D. A. Cucci, O. G. Crespillo, and M. Khaghani, "An analysis of a gyro-free inertial system for ins/gnss navigation," in Navigation Conference (ENC), 2016 European, pp. 1–7, IEEE, 2016.

[47] N. M. Barbour, "Inertial navigation sensors," tech. rep., Charles Stark Draper Lab Inc Cambridge Ma, 2010.

[48] I. Skog, J.-O. Nilsson, P. Händel, and A. Nehorai, "Inertial sensor arrays, maximum likelihood, and cramér–rao bound," IEEE Transactions on Signal Processing, vol. 64, no. 16, pp. 4218–4227, 2016.

[49] P. Mittendorfer and G. Cheng, "3d surface reconstruction for robotic body parts with artificial skins," in Intelligent Robots and Systems (IROS), 2012 IEEE/RSJ International Conference on, pp. 4505–4510, IEEE, 2012.